CLEARED FOR PUBLIC RELEASE
PL/PA 16 DEC 96

Sensor and Simulation Notes

Note 170

February 1973

Impedances and Field Distributions of Curved Parallel-Plate Transmission-Line Simulators

Tom K. Liu
Dikewood Corporation, Westwood Research Branch
Los Angeles, California 90024

Abstract

The impedances and field distributions of two curved parallel-plates are presented. In this report, the circular geometry is studied in detail and it is found that maximum field uniformity occurs when each plate substains an angle of 90° at the center of the circle.

PL 96-0974

I. Introduction

In the design of parallel-plate transmission-line simulators, it is desirable to achieve a maximum working volume inside which the electric field is with prescribed uniformity. Baum [1] carried out the calculations of impedances and field distributions of the TEM-mode for straight parallel-plate transmission-line simulators. In this note, we present a similar study of curved parallel-plate transmission-line simulators, and try to optimize the field uniformity for such a configuration. The particular geometry we analyze is two circular plates, as shown in Fig. 1. Such a study will provide physical insights into the general curved-plate problems and give useful results in EMP simulator design.

We approach this problem by means of conformal tranformations. Moon and Spencer [2] have provided a transformation which is proved to be useful for this circular geometry. Independently, we applied successive conformal transformations which have yielded the same results as that of Moon and Spencer. In Appendix A, the derivation of the final transformation formula is presented because this provides a better physical insight into this problem.

In Section II, the transformation is presented and the complex potential function is defined. From these expressions, we derive the equations for the electric field and impedance. In Section III, the geometry for the optimum field uniformity is found, and we present results for the potential, field and charge distribution, and the geometric impedance factor.

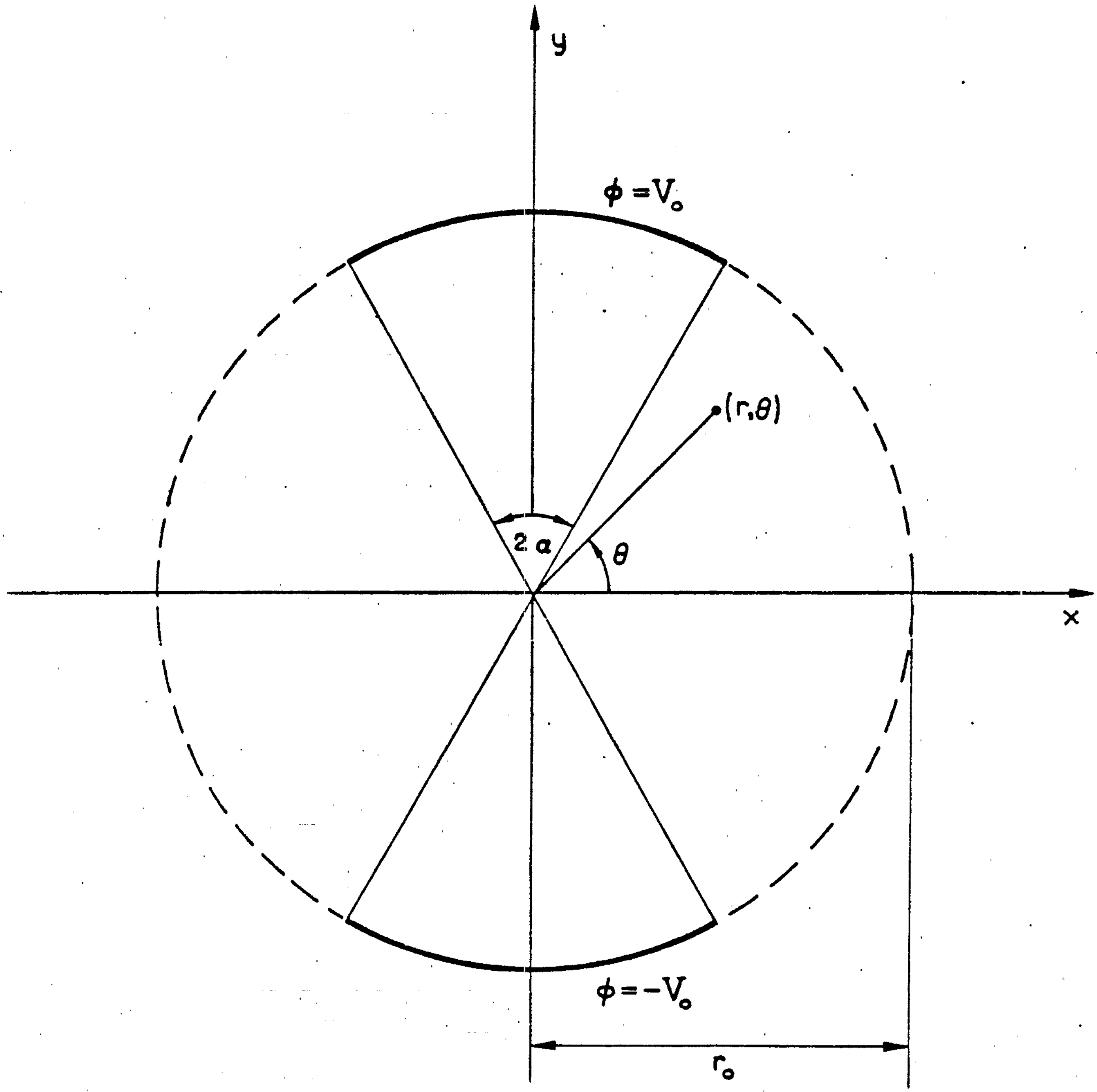

Fig. 1. A circular parallel-plate transmission-line simulator with plate angle 2α and radius r_o.

II. Mathematical Formulation

In this section, we make use of a transformation similar to that of No. J3 given by Moon and Spencer [2]. In Appendix A, we show that four successive conformal transformations provide the same result.

The transformation we use is

$$z = \frac{1+jm^{1/4}\ \mathrm{sn}(w|m)}{1-jm^{1/4}\ \mathrm{sn}(w|m)} \tag{1}$$

where

$$z = x + jy, \tag{2}$$

$$w = u + iv, \tag{3}$$

and $\mathrm{sn}(w|m)$ is a Jacobian elliptic function [3]. Transformation (1) differs slightly from that of Moon and Spencer and is illustrated schematically in Fig. 2. We shall show that the loci of z for $u = \pm K(m)$ are circular arcs.

Expanding $\mathrm{sn}(w|m)$ [3], we have

$$\mathrm{sn}(u + jv|m) = \frac{\mathrm{sn}(u|m)\mathrm{dn}(v|m_1)+j\ \mathrm{cn}(u|m)\mathrm{dn}(u|m)\mathrm{sn}(v|m_1)\mathrm{cn}(v|m_1)}{\mathrm{cn}^2(v|m_1)+m\ \mathrm{sn}^2(u|m)\mathrm{sn}^2(v|m_1)}, \tag{4}$$

where

$$m_1 = 1 - m. \tag{5}$$

It is noted that the parameters m and m_1 are associated with u and v, respectively. To simplify the notations, we suppress the parameters in the Jacobian functions sn, cn, and dn. Thus, (4) becomes

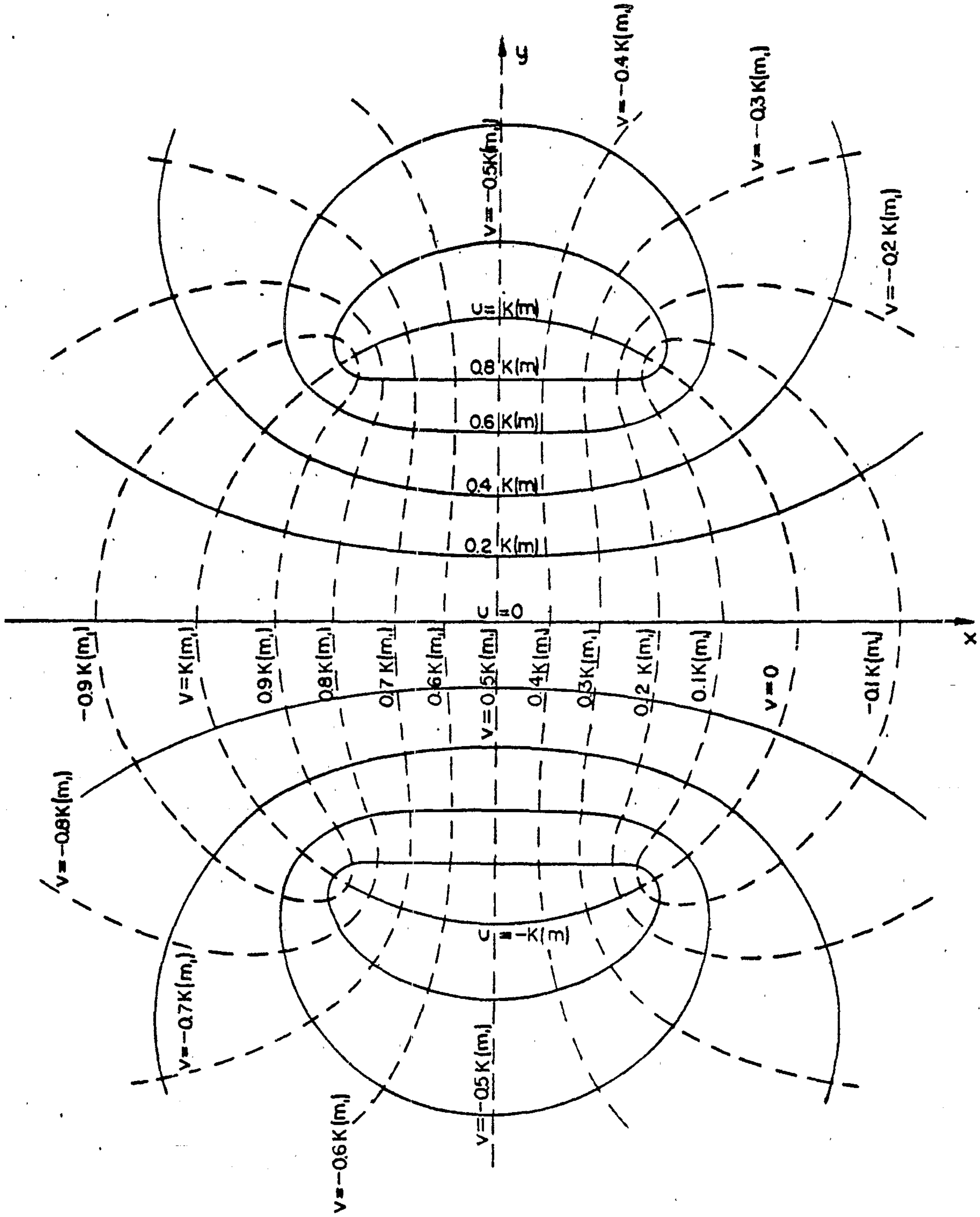

Fig. 2. Complex potential w in the complex z-plane $w = u + jv$, $z = x + jy$.

$$\mathrm{sn}(u + iv|m) = \frac{\mathrm{sn}\ u\ \mathrm{dn}\ v + j\ \mathrm{cn}\ u\ \mathrm{dn}\ u\ \mathrm{sn}\ v\ \mathrm{cn}\ v}{\mathrm{cn}^2 v + m\ \mathrm{sn}^2 u\ \mathrm{sn}^2 v}\ . \qquad (6)$$

From (1) and (6), we obtain

$$x = T\Gamma^{-1} \qquad (7)$$

and

$$y = 2\Lambda\ \mathrm{sn}\ u\ \mathrm{dn}\ v \cdot (m^{1/4}\ \Gamma)^{-1}, \qquad (8)$$

where

$$\Lambda = 1 - \mathrm{dn}^2 u\ \mathrm{sn}^2 v$$

$$\Gamma = \mathrm{sn}^2 u\ \mathrm{dn}^2 v + (\Lambda m^{-1/4} + \mathrm{cn}\ u\ \mathrm{dn}\ u\ \mathrm{sn}\ v\ \mathrm{cn}\ v)^2$$

and

$$T = \Lambda^2\ m^{-1/2} - [(\mathrm{cn}\ u\ \mathrm{dn}\ u\ \mathrm{sn}\ v\ \mathrm{cn}\ v)^2 + \mathrm{sn}^2 u\ \mathrm{dn}^2 v]. \qquad (9)$$

It is to be noted that the corresponding expressions in Moon and Spencer contain an error.

From (7), (8) and (9), we can show that, for $u = \pm K(m)$, where $K(m)$ is the complete elliptic integral of the first kind, the following relationship is obtained:

$$x^2 + y^2 = 1.$$

This means that $u = \pm K(m)$ defines a pair of circular arcs with a unity radius.

It is further observed from Moon and Spencer that one edge of the circular arc is at the values $u = K(m)$, $v = 0$. This defines the half angle of the arc, α, such that

$$\tan \alpha = \frac{1-m^{1/2}}{2m^{1/4}} . \tag{10}$$

From above, it is clear that (1) describes the potential distribution for two circular parallel-plates biased at equal but opposite potentials $\pm K(m)$, and w is the complex potential function. When normalizing the plate potentials to $\pm V_o$, we define

$$w_n = u_n + j\, v_n = \frac{V_o}{K(m)}\, w, \tag{11}$$

which is the normalized complex potential function.

To calculate the electric field for this normalized case, we make use of the following expression [4], [5]:

$$\frac{dw_n}{dz} = \frac{\partial u_n}{\partial x} - j\, \frac{\partial u_n}{\partial y} ,$$

i.e., the complex conjugate of the normalized electric field, $\overline{E}$, is given by

$$\overline{E} = E_x - j\, E_y = \frac{dw_n}{dz} , \tag{12}$$

i.e.,

$$E_x = \mathrm{Re}\left(\frac{dw_n}{dz}\right) ,$$

and

$$E_y = -\mathrm{Im}\left(\frac{dw_n}{dz}\right) .$$

From (1) and (11), we have

$$\mathrm{sn}(K(m)V_o^{-1}\, w_n|m) = -\frac{j}{m^{1/4}}\,\frac{z-1}{z+1}\ . \tag{13}$$

Let

$$\nu(z) = \mathrm{sn}(K(m)V_o^{-1}\, w_n|m), \tag{14}$$

then

$$w_n = \frac{V_o}{K(m)}\,\mathrm{sn}^{-1}(\nu|m) = \frac{V_o}{K(m)}\int_o^{\nu}\frac{d\lambda}{\sqrt{(1-\lambda^2)(1-m\lambda^2)}}\ . \tag{15}$$

Now

$$\frac{dw_n}{dz} = \frac{dw_n}{d\nu}\cdot\frac{d\nu}{dz}$$

$$= \frac{V_o}{K(m)\sqrt{(1-\nu^2)(1-m\nu^2)}}\cdot\frac{-2j}{m^{1/4}(z+1)^2}\ .$$

Thus,

$$\overline{E} = \frac{2jV_o}{K(m)(1+m^{1/2})}\left\{z^4 + 2\left[1 - 2\left(\frac{1-m^{1/2}}{1+m^{1/2}}\right)^2\right]z^2 + 1\right\}^{-1/2}\ . \tag{16}$$

We now define

$$E_o = \frac{2V_o}{K(m)(1+m^{1/2})}\ , \tag{17}$$

which is the value of the field at $z = 0$. A dimensionless factor f_E can be defined

$$f_E = r_oE_o/V_o \tag{18}$$

which is a measure of the electric field at $z = 0$ when the plates are biased at ±1 volts.

The geometric impedance factor, f_g, is given by [4]

$$f_g = \frac{\Delta u}{\Delta v} ,$$

where Δu is the change in the potential function between the plates and Δv is the change in the stream function on a path encircling one plate. From Fig. 2, we obtain

$$f_g = K(m)/K(m_1). \tag{19}$$

As is in Baum's work [1], this quantity is defined to relate the line impedance Z_L to the wave impedance Z, such that

$$Z_L = f_g Z. \tag{20}$$

The capacitance per unit length of the line is

$$C = \varepsilon/f_g, \tag{21}$$

and the inductance per unit length is

$$L = \mu f_g. \tag{22}$$

III. Results

We shall first present the procedures in obtaining the configuration for optimum field uniformity. We can expand the electric field at z, $\bar{E}(z)$, in a Taylor series about z = 0,

$$\bar{E}(z) = \sum_{n=0}^{\infty} \frac{z^n}{n!} \frac{d^n\bar{E}}{dz^n}(0)$$

For higher field uniformity, i.e., for $\bar{E}(z)$ being closer to $\bar{E}(0)$, more higher terms in the series should vanish. From the symmetry of the problem, all odd derivatives of $\bar{E}(z)$ at z = 0 are zero. In this structure, we have only one degree of freedom, namely, the half angle of the plate, α, hence, we expect that we can only set the second derivative of $\bar{E}(z)$ at z = 0 to be zero. This leaves the resulting field to be of the following forms:

$$\bar{E}(z) = \bar{E}(0) + \frac{d^4\bar{E}}{dz^4}(0)\,\frac{z^4}{4!} + \text{higher order terms.} \tag{23}$$

From (16) and (17), the first derivative of $\bar{E}(z)$ is,

$$\frac{d\bar{E}}{dz}(z) = jE_o \frac{2z^3+2[1-2(1-m^{1/2})^2(1+m^{1/2})^{-2}]z}{\{z^4+2[1-2(1-m^{1/2})^2(1+m^{1/2})^{-2}]z^2+1\}^{3/2}} ,$$

and $\frac{d\bar{E}}{dz}(0) = 0$ as expected.

The second derivative gives

$$\frac{d^2\bar{E}}{dz^2}(0) = jE_o \frac{6z^2+2[1-2(1-m^{1/2})^2(1+m^{1/2})^{-2}]}{\{z^4+2[1-2(1-m^{1/2})^2(1+m^{1/2})^{-2}]z^2+1\}^{3/2}}$$

$$-jE_o \frac{3[2z^3+2[1-2(1-m^{1/2})^2(1+m^{1/2})^{-2}]z]^2}{\{z^4+2[1-2(1-m^{1/2})^2(1+m^{1/2})^{-2}]z^2+1\}^{5/2}}$$

and

$$\frac{d^2\overline{E}}{dz^2}(0) = 2jE_o\left[1 - 2\left(\frac{1-m^{1/2}}{1+m^{1/2}}\right)^2\right].$$

Setting this second derivative equal to zero, we get,

$$m^{1/2} = \frac{\sqrt{2}-1}{\sqrt{2}+1} = 3 - 2\sqrt{2} = 0.17157. \tag{24}$$

From (10), the half angle for the optimum field uniformity, α_{opt}, may be shown to be

$$\alpha_{opt} = \tan^{-1} 1 = 45^o. \tag{25}$$

In Fig. 3, we present the field and potential distribution for the optimum case, i.e., $\alpha = 45^o$. It is observed that the potential is reasonably constant up to a radius of $\frac{1}{2} r_o$, where r_o is the radius of the circular plates. There is a high concentration of field lines near the edge of the plate, as expected. For comparison, we also present the same plots for the two cases $\alpha = 30^o$ and $\alpha = 60^o$ in Fig. 4 and Fig. 5, respectively. Indeed, we see that $\alpha = 45^o$ has higher field uniformity.

The electric field plots are presented normalized with respect to the electric field at the center, E_o. In Fig. 6, we show the values of f_E, as defined by (18), as a function of the half plate angle α. The values f_E is also tabulated in Table I. For $\alpha = \alpha_{opt} = 45^o$, the normalized electric field is plotted against the normalized radius r/r_o in Fig. 7, for various values of θ (θ is defined in Fig. 1). It is observed that there is an even symmetry about $\theta = 45^o$ for E_y, the y-component of the electric field, and an odd symmetry about $\theta = 45^o$ for E_x, the x-component of the electric field. The electric field is infinite at the edge of the plate, i.e., $r/r_o = 1$ and $\theta = 45^o$. The alternative electric field plot against θ for various r/r_o values is

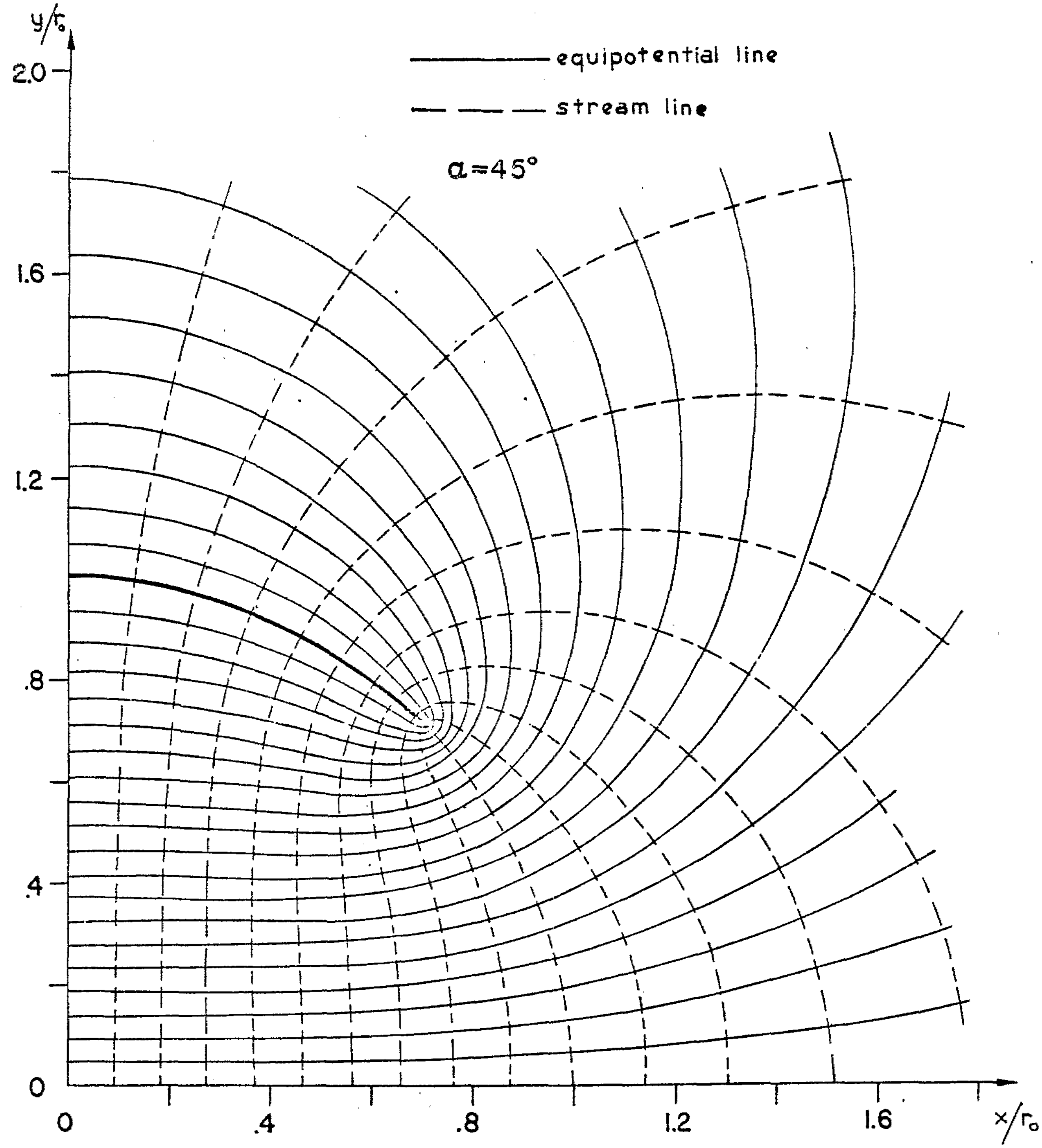

Fig. 3. The field and potential distributions for $\alpha = \alpha_{opt} = 45^{\circ}$.

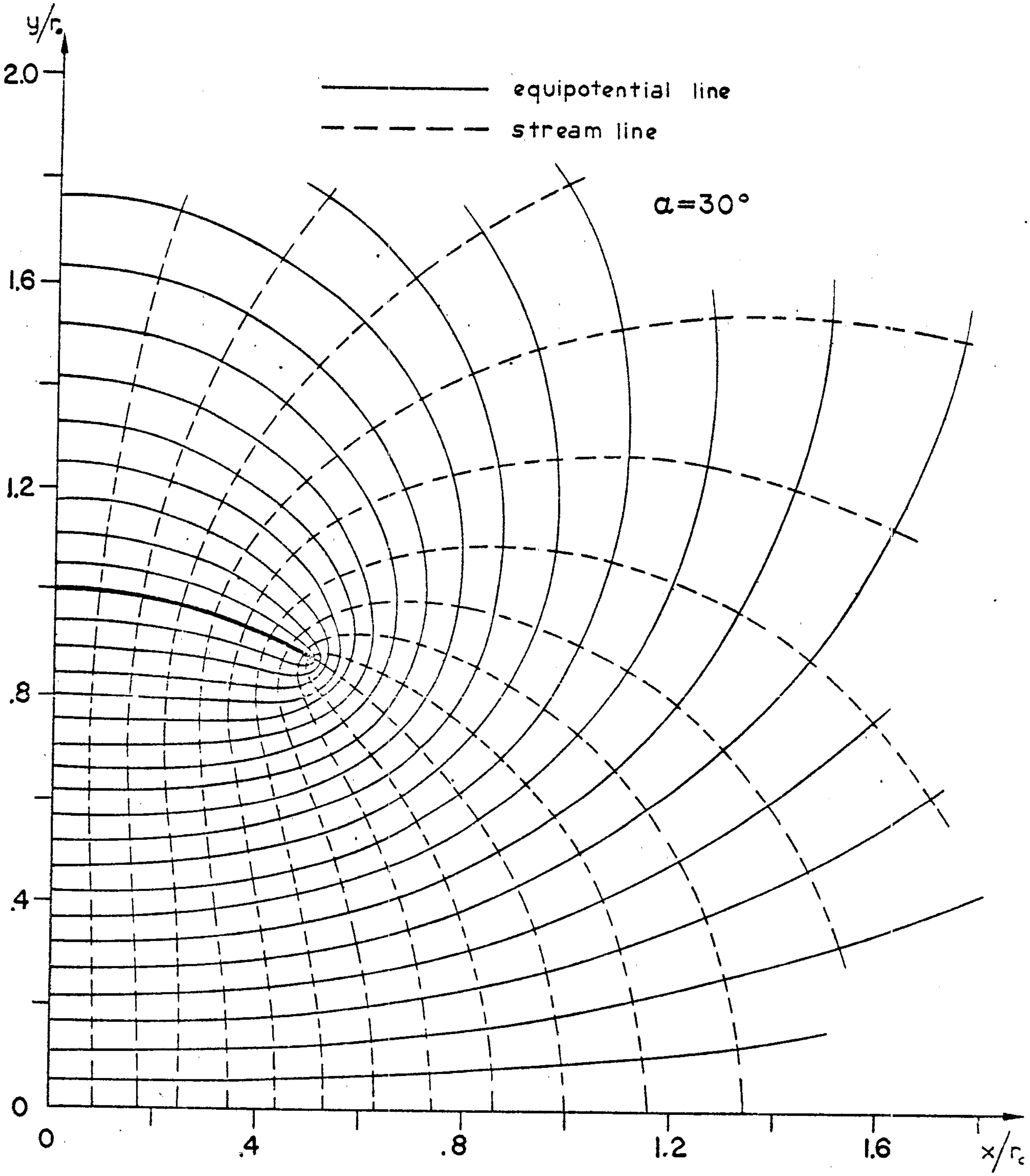

Fig. 4. The field and potential distributions for $\alpha = 30^{\circ}$.

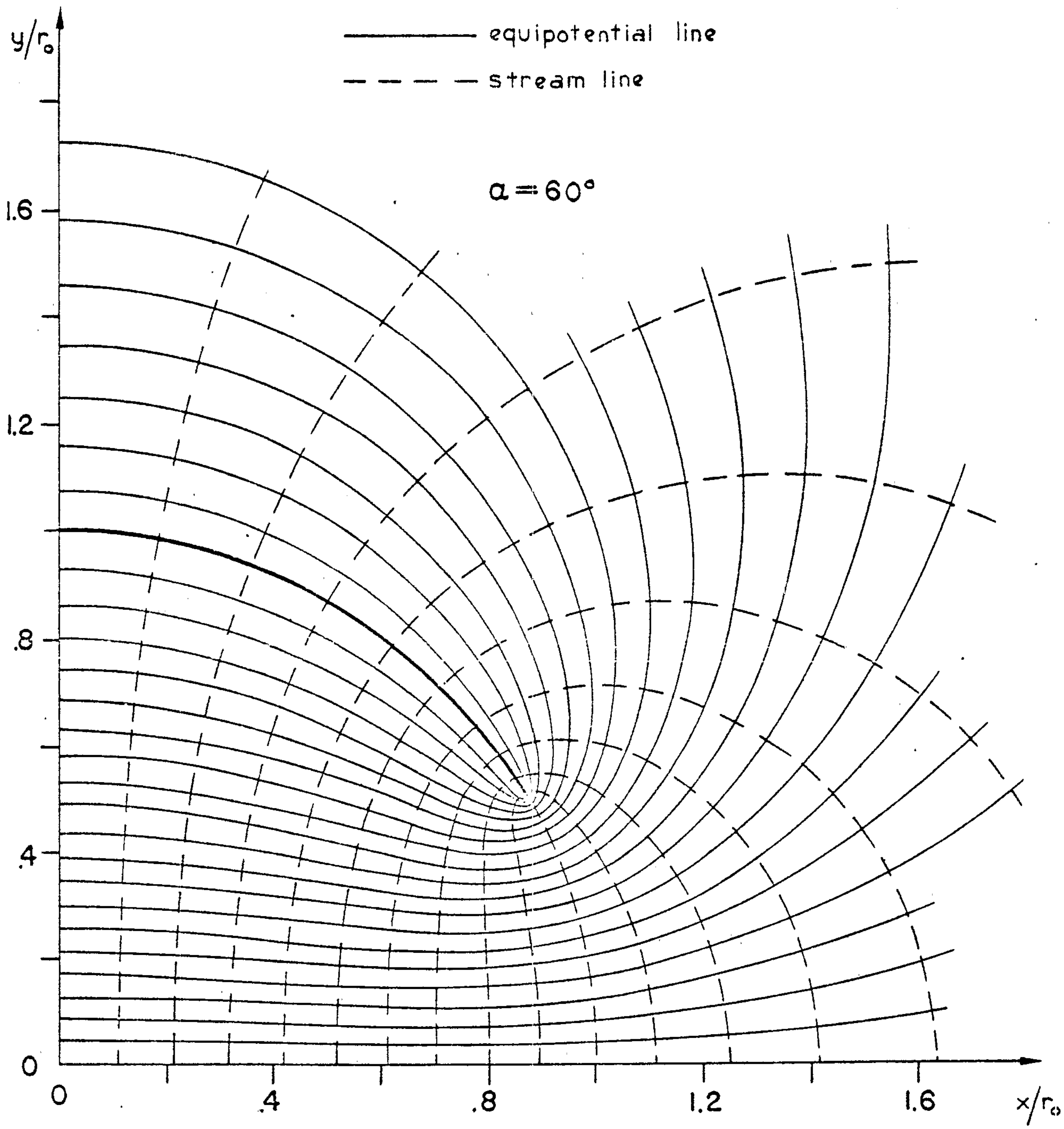

Fig. 5. The field and potential distributions for $\alpha = 60^{\circ}$.

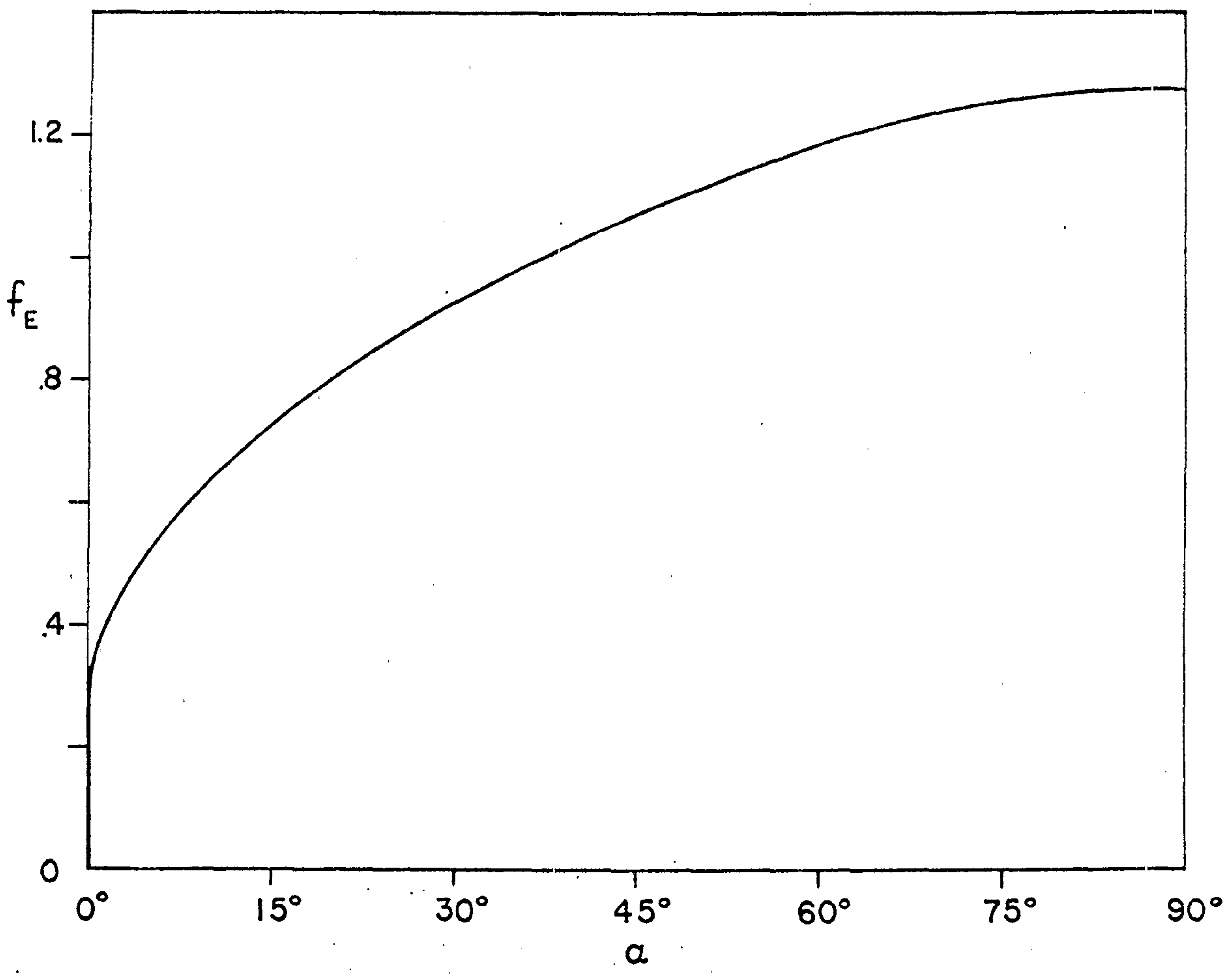

Fig. 6. The electric field at the center versus the half angle of the plate. The electric field is normalized with respect to V_o/r_o, where V_o is the biasing voltage on the plate and r_o is the radius of the plate.

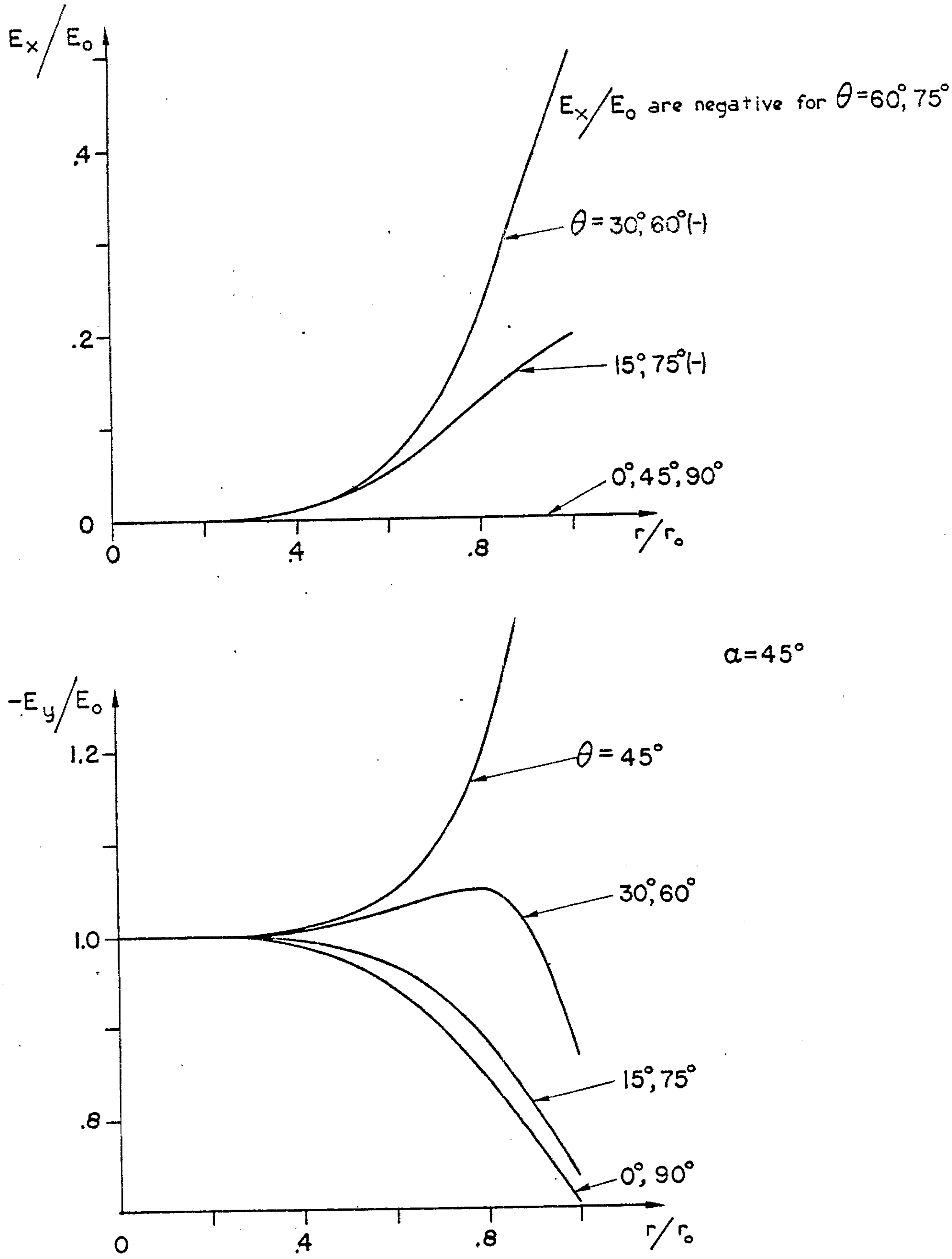

Fig. 7. Normalized electric field versus radius for $\alpha = 45^{\circ}$. The y-components of the electric field, E_y, are all negative, whereas the x-components, E_x, are negative for $\theta > 45^{\circ}$.

Table I. Values of $f_E = r_o E_o / V_o$

α (degree)	f_E	α (degree)	f_E	α (degree)	f_E
0	0.	30	0.92742	60	1.18642
1	0.36799	31	0.93900	61	1.19208
2	0.42170	32	0.95027	62	1.19756
3	0.46097	33	0.96137	63	1.20285
4	0.49349	34	0.97226	64	1.20795
5	0.52196	35	0.98294	65	1.21286
6	0.54767	36	0.99341	66	1.21758
7	0.57136	37	1.00368	67	1.22211
8	0.59350	38	1.01375	68	1.22645
9	0.61438	39	1.02361	69	1.23059
10	0.63424	40	1.03328	70	1.23455
11	0.65323	41	1.04275	71	1.23831
12	0.67146	42	1.05203	72	1.24189
13	0.68905	43	1.06112	73	1.24527
14	0.70605	44	1.07001	74	1.24846
15	0.72253	45	1.07871	75	1.25145
16	0.73853	46	1.08721	76	1.25426
17	0.75411	47	1.09553	77	1.25687
18	0.76928	48	1.10366	78	1.25929
19	0.78409	49	1.11159	79	1.26152
20	0.79855	50	1.11934	80	1.26355
21	0.81268	51	1.12690	81	1.26539
22	0.82650	52	1.13427	82	1.26704
23	0.84003	53	1.14144	83	1.26849
24	0.85328	54	1.14844	84	1.26975
25	0.86626	55	1.15524	85	1.27082
26	0.87900	56	1.16185	86	1.27169
27	0.89145	57	1.16828	87	1.27237
28	0.90367	58	1.17451	88	1.27285
29	0.91566	59	1.18056	89	1.27314
30	0.92742	60	1.18642	90	1.27324

presented in Fig. 8. The vector nature of the field distribution is illustrated in Fig. 9, which gives some insight into the field behavior.

By studying the electric field quantities, we can determine the maximum radius inside which the electric field is within a certain percentage of the field at the center. We define the electric field variation as

$$\frac{|\Delta\bar{E}|}{|\bar{E}(0)|} = \frac{|\bar{E}(z)-\bar{E}(0)|}{|\bar{E}(0)|} \tag{26}$$

In Table II, for $\alpha = \alpha_{opt} = 45^{o}$ we present $|\Delta\bar{E}|/|\bar{E}(0)|$ versus the maximum allowable radius.

Table II. Maximum allowable radius for a given electric field variation. $\alpha = \alpha_{opt} = 45^{o}$

$\frac{\lvert\Delta\bar{E}\rvert}{\lvert E_o\rvert} \times 100\%$	radius r
1%	$0.35\ r_o$
2%	$0.45\ r_o$
5%	$0.55\ r_o$
10%	$0.65\ r_o$

The charge density σ on the conducting plate is presented in Fig. 10 as a function of θ for the case $\alpha = \alpha_{opt} = 45^{o}$. The charge density is proportional to the normal electric field on the plate and we normalize it with respect to E_o/ε.

The geometric impedance factor fg is presented in Fig. 11 as well as tabulated in Table III. It is interesting to compare this with two straight parallel plates of width 2a and separated by 2b [1], [6]. In Fig. 12, we present the relationship between the straight parallel-plate geometry and the curved parallel-plate geometry for various fg values.

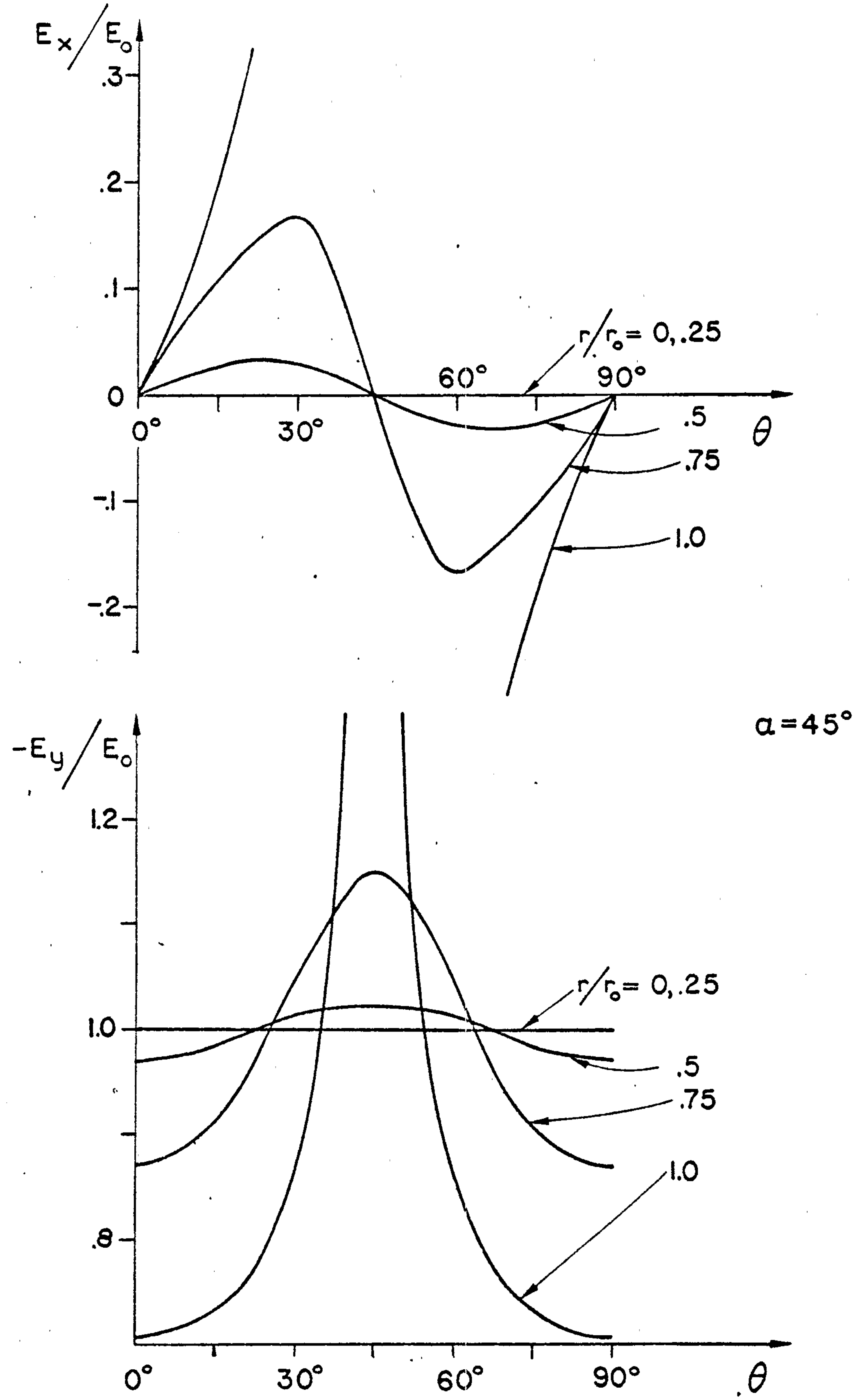

Fig. 8. Normalized electric field versus angle θ for $\alpha = 45^{\circ}$. The E_y values are all negative.

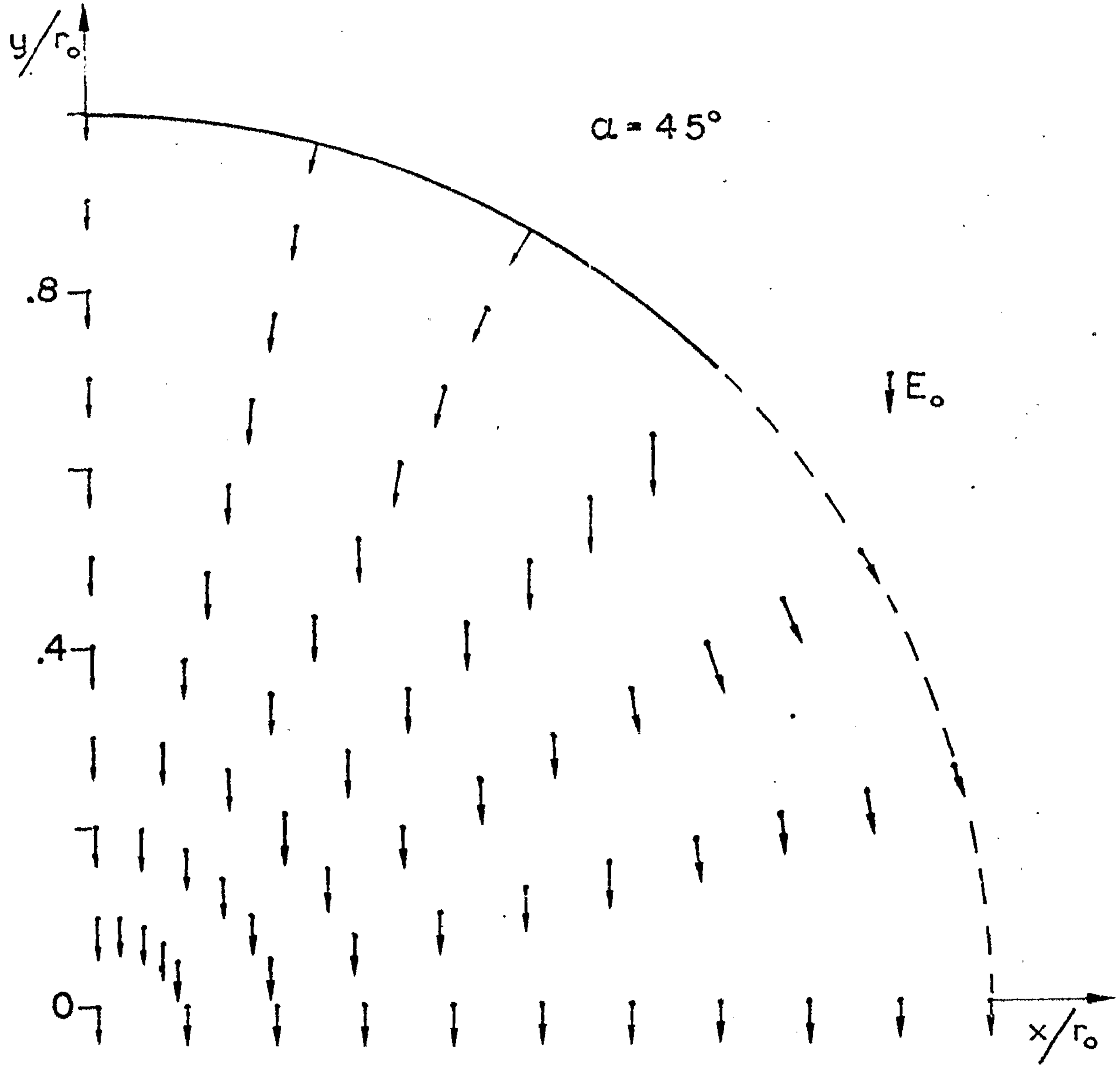

Fig. 9. The electric field distributions inside the circular region. The lengths of the vectors are proportional to the magnitude of the electric field.

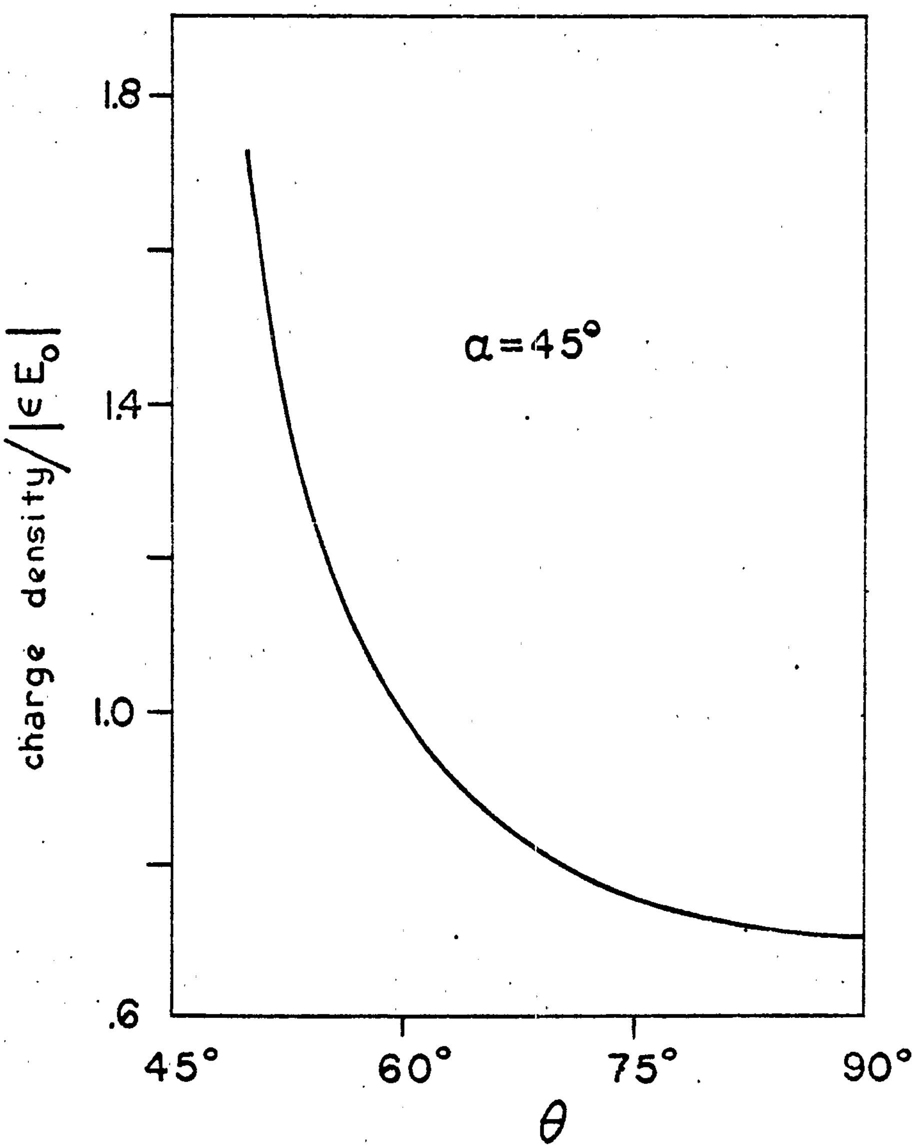

Fig. 10. Normalized charge density on the plate for $\alpha = 45^{\circ}$.

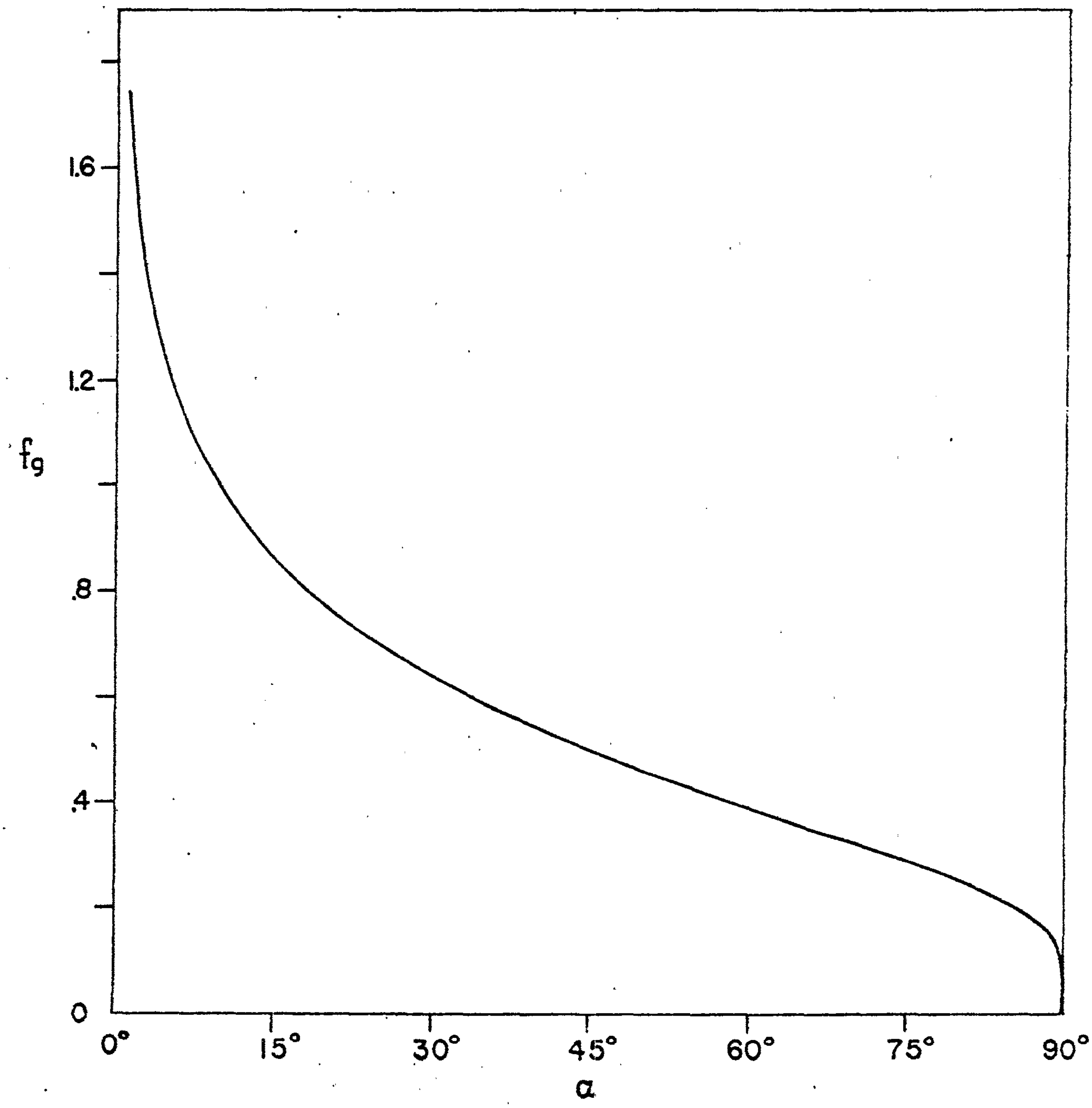

Fig. 11. Geometric factor versus α.

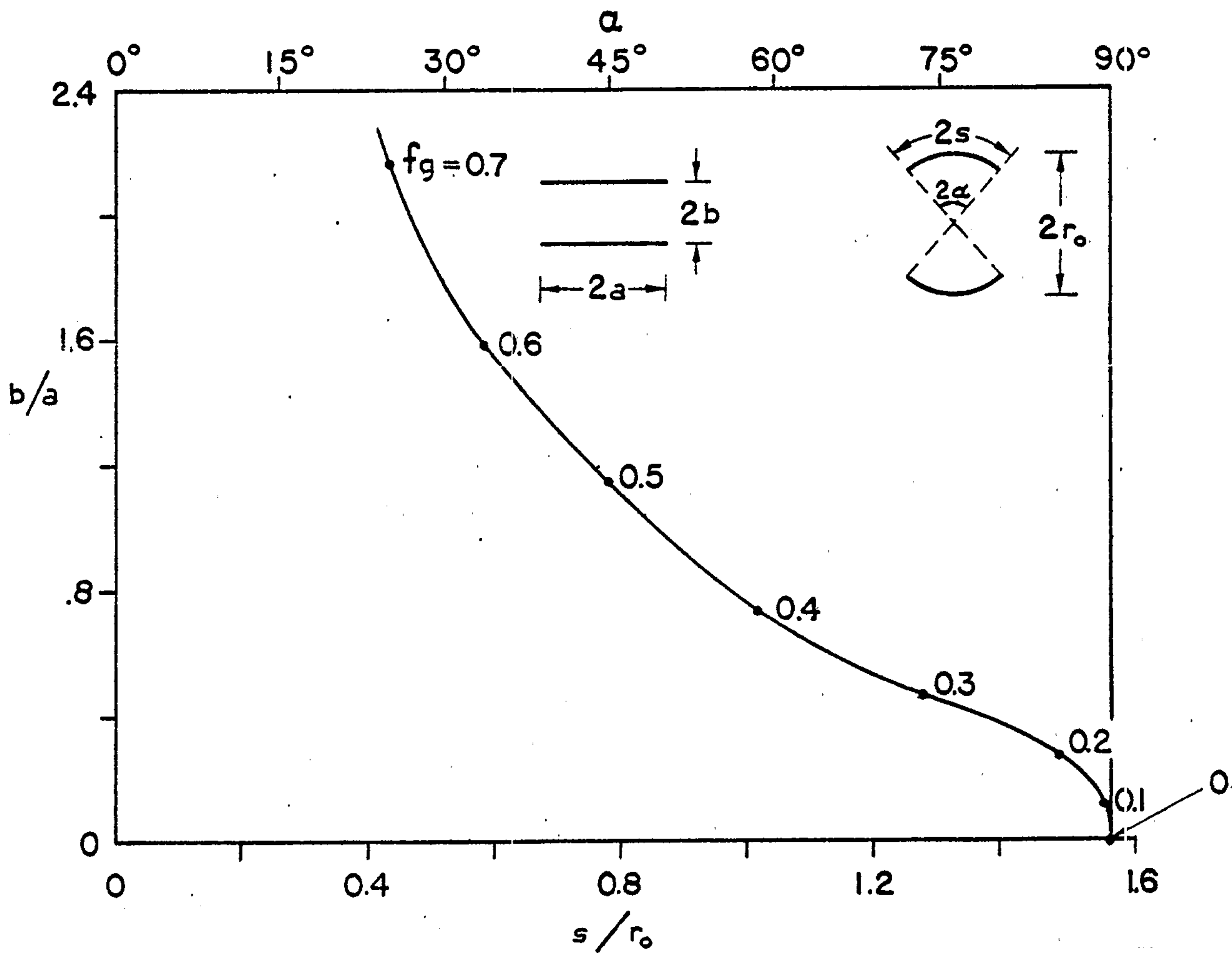

Fig. 12. Relationship between the straight parallel-plate geometry and the circular parallel-plate geometry for various f_g values.

Table III. Geometric impedance factor f_g.

α (degree)	f_g	α (degree)	f_g	α (degree)	f_g
0	∞	30	0.63963	60	0.39085
1	1.72985	31	0.62865	61	0.38406
2	1.50919	32	0.61799	62	0.37730
3	1.38009	33	0.60761	63	0.37056
4	1.28846	34	0.59750	64	0.36383
5	1.21736	35	0.58765	65	0.35711
6	1.15924	36	0.57803	66	0.35040
7	1.11006	37	0.56863	67	0.34368
8	1.06744	38	0.55944	68	0.33695
9	1.02981	39	0.55045	69	0.33020
10	0.99611	40	0.54164	70	0.32342
11	0.96561	41	0.53301	71	0.31660
12	0.93771	42	0.52454	72	0.30972
13	0.91204	43	0.51622	73	0.30279
14	0.88823	44	0.50804	74	0.29578
15	0.86603	45	0.50000	75	0.28868
16	0.84523	46	0.49209	76	0.28146
17	0.82566	47	0.48429	77	0.27411
18	0.80717	48	0.47661	78	0.26660
19	0.78965	49	0.46904	79	0.25891
20	0.77300	50	0.46156	80	0.25098
21	0.75712	51	0.45417	81	0.24276
22	0.74195	52	0.44687	82	0.23421
23	0.72742	53	0.43965	83	0.22521
24	0.71347	54	0.43251	84	0.21566
25	0.70006	55	0.42543	85	0.20536
26	0.68714	56	0.41841	86	0.19403
27	0.67466	57	0.41145	87	0.18115
28	0.66261	58	0.40454	88	0.16565
29	0.65094	59	0.39768	89	0.14452
30	0.63963	60	0.39085	90	0.

IV. Conclusions

We have presented, in this report, the impedances and field distributions of two circular parallel-plate transmission-line. It is found that for the plate angle of 90°, we have the optimum field uniformity.

Appendix A. Derivation

We show, in this appendix, that the formulas presented in the text can be derived using four successive conformal transformations. This process provides more physical insights into the problem considered in the text.

The use of a logarithmic transformation maps a quadrant of a circle into a semi-infinite strip, which, on the application of a sine transformation, is mapped into a straight line. Using the Schwarz-Christoffel transformation, this later configuration is mapped into a rectangle with simple boundary conditions, the solution of which is readily obtained.

Because of the symmetry of the configuration, we concentrate on only one quadrant of the circle. The corresponding points in all the planes are identified by the same parenthesized number, e.g., point (3) in the w_3-plane corresponds to point (3) in the z-plane as a result of the transformations. The process of the successive transformation is illustrated in Fig. A.1.

Using the logarithmic transformation [7], the first quadrant of the z-plane is mapped into an infinite strip in the w_1-plane. The interior of the unit circle in the z-plane now transforms into the upper half strip, whereas the exterior, the lower half strip. In the w_1-plane, the configuration is symmetric about the $v_1 = 0$ axis and we continue the transformation for only the upper half strip, i.e., the interior of the circle. The sine transformation opens up the strip into a line in the w_2-plane. The configuration in the w_2-plane is similar to the one given by Collin [8], who uses the Schwarz-Christoffel transformation to obtain the configuration in the w_3-plane. The potential function for this final form is readily calculated.

The transformations are summarized in the following:

$$w_1 = 2j \ln z + \pi/2, \tag{A.1}$$

$$w_2 = (2p)^{-1}(\sin w_1 - 1), \tag{A.2}$$

and

$$w_3 = -j[K(p_1)]^{-1} \operatorname{sn}^{-1}(\sqrt{-w_2}, p) + 1 + jK(p)/K(p_1), \tag{A.3}$$

$$z \xrightarrow{\;w_1 = 2j\ \ln z + \pi/2\;} w_1 \xrightarrow[\;p = \cos^2\alpha\;]{\;w_2 = (\sin w_1 - 1)/2p\;} w_2 \xrightarrow[\;p_1 = 1 - p\;]{\;w_3 = \frac{-j}{K(p_1)}\ \mathrm{sn}^{-1}(\sqrt{-w_2}\,|p) + 1 + \frac{jK(p)}{K(p_1)}\;} w_3$$

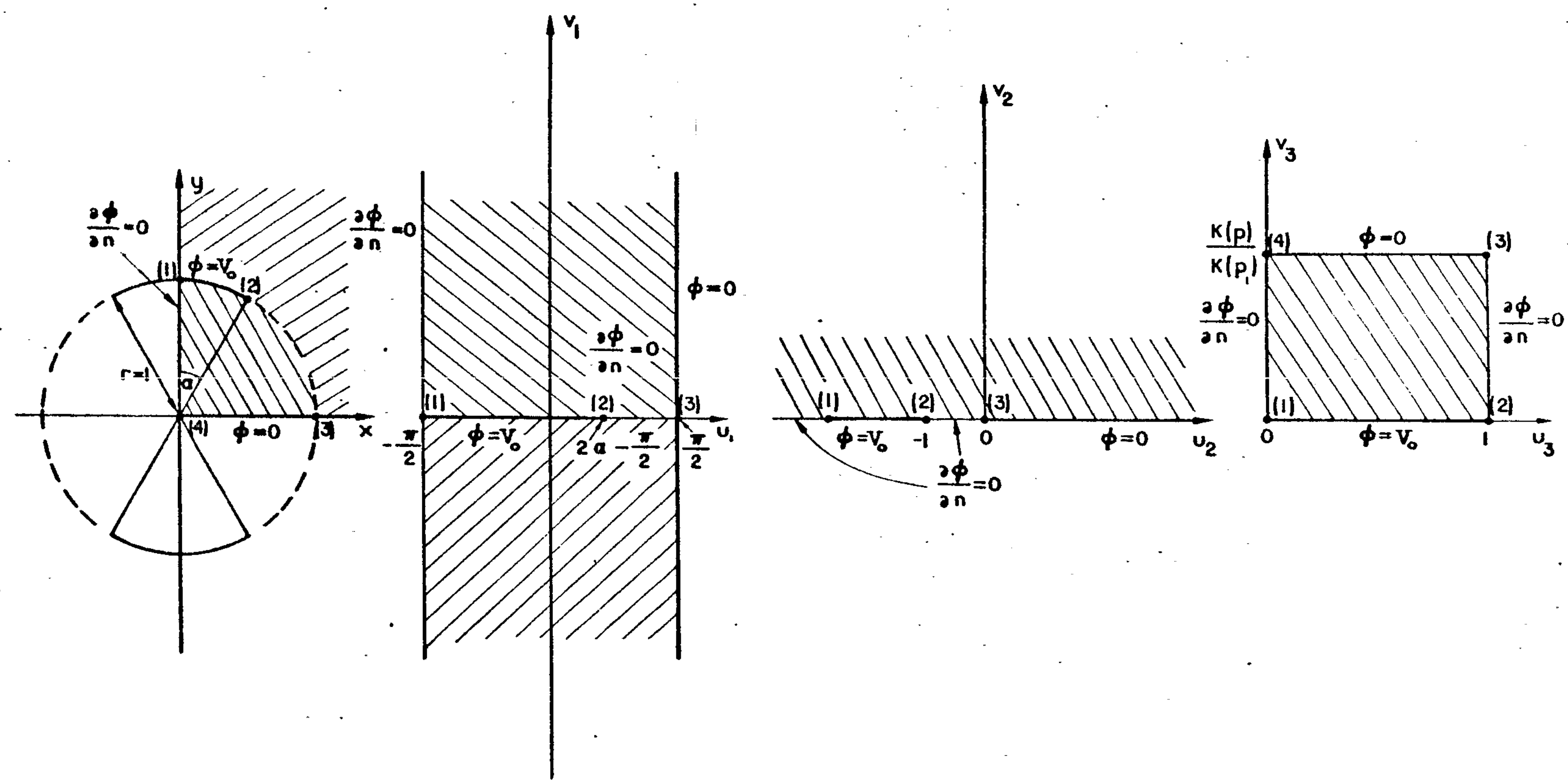

Fig. A.1. The four-step successive conformal transformation.

where

$$p = \cos^2\alpha, \tag{A.4}$$

and

$$p_1 = 1 - p. \tag{A.5}$$

K(p) is the complete elliptic integral of the first kind with the parameter p.

The v_3 = constant contours are the equipotential lines in the w_3-plane. The potentials in the w_3-plane, when the plates are biased at $\pm V_o$ are given by

$$\phi = V_o\left[1 - \frac{K(p_1)}{K(p)}\, v_3\right],$$

and we define the complex potential function as

$$F(w_3) = V_o\left[1 + j\,\frac{K(p_1)}{K(p)}\, w_3\right], \tag{A.6}$$

so that the complex conjugate of the electric field is given by

$$\overline{E} = E_x - jE_y = \frac{dF}{dz} = jV_o\,\frac{K(p_1)}{K(p)}\,\frac{dw_3}{dz}\ . \tag{A.7}$$

It can be readily shown that

$$\sqrt{-w_2} = (4p)^{-1/2}(z - \frac{1}{z}),$$

hence

$$\overline{E} = \frac{2jV_o}{K(p)}\left\{z^4 + 2[2p - 1]z^2 + 1\right\}^{-1/2}\ . \tag{A.8}$$

Comparing with (16), for the same z variation, we demand

$$2p - 1 = 1 - 2\left(\frac{1-m^{1/2}}{1+m^{1/2}}\right)^2,$$

i.e.,

$$p = \frac{4m^{1/2}}{[1+m^{1/2}]^2} . \tag{A.9}$$

We can check the consistency of this relationship by comparing the formulas for the half angle of the plate, α. From (A.4),

$$\cos \alpha = p^{1/2} = \frac{2m^{1/4}}{1+m^{1/2}}$$

hence

$$\tan \alpha = \frac{1-m^{1/2}}{2m^{1/4}}$$

which is identical to (10).

It remains to check the amplitude of the field. Comparing (A.8) and (18), we want to prove that

$$K(p) = K\left(\frac{4m^{1/2}}{(1+m^{1/2})^2}\right) = K(m)(1 + m^{1/2}).$$

Indeed, such an identity can be obtained from Table VI.5 of Jahnke and Emde [9].

Thus, the transformation (1) as given by Moon and Spencer can be obtained by four successive conformal transformations.

Acknowledgement

The author is grateful that Dr. C. E. Baum who suggested the use of the transformation in Moon and Spencer, which subsequently is proved to be the same as the successive transformations that the author was investigating. Special thanks are expressed to Drs. Kelvin S. H. Lee and Lennart Marin for their numerous suggestions.

References

1. C. E. Baum, "Impedances and field distributions for parallel plate transmission line simulators," Sensor and Simulation Note 21, June 1966.
2. P. Moon and D. E. Spencer, Field Theory Handbook, Springer-Verlag, 1961.
3. M. Abramowitz and I. A. Stegun, Handbook of Mathematical Functions, National Bureau of Standards, Applied Mathematics Series 55, 1970.
4. C. E. Baum, "General principles for the design of ATLAS I and II, Part V," Sensor and Simulation Note 148, May 1972.
5. W. R. Smythe, Static and Dynamic Electricity, McGraw-Hill, 1950.
6. T. L. Brown and K. D. Granzow, "A parametric study of two parallel-plate transmission line simulators of EMP Sensor and Simulation Note 21," Sensor and Simulation Note 52, April 1968.
7. R. V. Churchill, Introduction to Complex Variables and Applications, McGraw-Hill, 1948.
8. R. E. Collin, Field Theory of Guided Waves, McGraw-Hill, 1960.
9. E. Jahnke and F. Emde, Table of Functions, Dover, 1945.